Available online at www.CivileJournal.org

Civil Engineering Journal

(E-ISSN: 2476-3055; ISSN: 2676-6957)

Vol. 11, No. 02, February, 2025

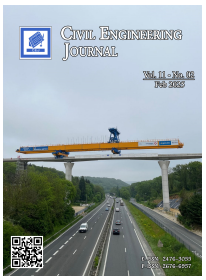

A Theoretical Pore Network Model for the Soil–Water Characteristic Curve and Hysteresis in Unsaturated Soils

Angela V. Gómez [1*]

[1] *Civil Engineering Program, Mariana University, Pasto, Colombia.*

Received 30 September 2024; Revised 15 January 2025; Accepted 22 January 2025; Published 01 February 2025

Abstract

This study presents a novel approach to modeling the soil–water characteristic curve in unsaturated soils, employing Monte Carlo simulations to capture the complex behavior of the pore network. The primary objective is to develop an alternative method to represent the hysteretic nature of the soil–water characteristic curve, which is critical for understanding unsaturated soil behavior in various engineering applications. The proposed approach conceptualizes soil as a network of interconnected pores, where each pore interacts with its nearest neighbors. Monte Carlo simulations are used to model the pore-filling distribution as a function of pressure differences during drying and wetting cycles. The model effectively reproduces the characteristic hysteresis curves associated with the hydraulic and mechanical processes in unsaturated soils. A key finding is that the simulated soil–water characteristic curve captures the impact of pore-scale interactions and reflects the complex hysteresis effects observed in experimental data. The novelty of this work lies in integrating pore network modeling with Monte Carlo simulations, addressing limitations of traditional models and offering a more accurate representation of unsaturated soil behavior. While the model has not yet undergone experimental validation, it provides valuable insights into the dynamics of soil moisture retention and serves as a foundation for future experimental testing and refinement of soil–water models.

Keywords: Unsaturated Soil; Hysteresis; Monte Carlo; Statistics; Ising Model.

1. Introduction

Unsaturated soils are fundamental to a wide range of geotechnical and engineering applications. Unlike saturated soils, where properties such as permeability, compression index, and Young's modulus are often treated as constants, these properties in unsaturated soils vary significantly with the degree of saturation [1]. This variability has prompted the development of soil property functions to characterize and predict soil behavior under unsaturated conditions. Among these, the soil–water characteristic curve (SWCC) has emerged as a cornerstone for estimating critical unsaturated soil properties [2], including hydraulic conductivity, shear strength [3], and deformation [4].

The SWCC describes the relationship between soil suction and water content, with distinct drying and wetting paths that define critical points such as the air entry value (AEV), residual water content (ψ_r), and the water entry value (ψ_w). Consequently, the SWCC is inherently hysteretic—its behavior depends not only on the applied suction but also on the history of wetting and drying cycles [5]. This hysteresis is primarily caused by pore-scale phenomena, such as the "ink bottle" effect and variability in the contact angle of water within pores [6, 7]. Understanding and accurately modeling hysteresis is crucial for predicting unsaturated soil behavior in practical applications, as it significantly affects flow, deformation, and strength properties.

* Corresponding author: avgomeza@umariana.edu.co

http://dx.doi.org/10.28991/CEJ-2025-011-02-021

In Figure 1, the typical SWCC is presented, depicting the distinct drying and wetting paths of unsaturated soils. The air entry value (ψ_a) is identified as the point at which air begins to enter the soil pores during drainage or is expelled during the wetting process. Initially, as soil suction (ψ) increases from zero to ψ_a, the water content (θ_w) remains relatively constant. However, beyond ψ_a, further increases in suction result in a gradual decline in water content until the residual water content (θ_r) is reached, indicating the discontinuity of the water phase within the soil matrix. The suction corresponding to θ_r is known as the residual soil suction (ψ_r). Moreover, the water entry value (ψ_w) is defined as the matric suction at which the water content of the soil begins to rise significantly during the wetting process. This understanding of the SWCC is fundamental for predicting the hydraulic behavior of unsaturated soils, which is critical in various geotechnical and environmental engineering applications [8, 9].

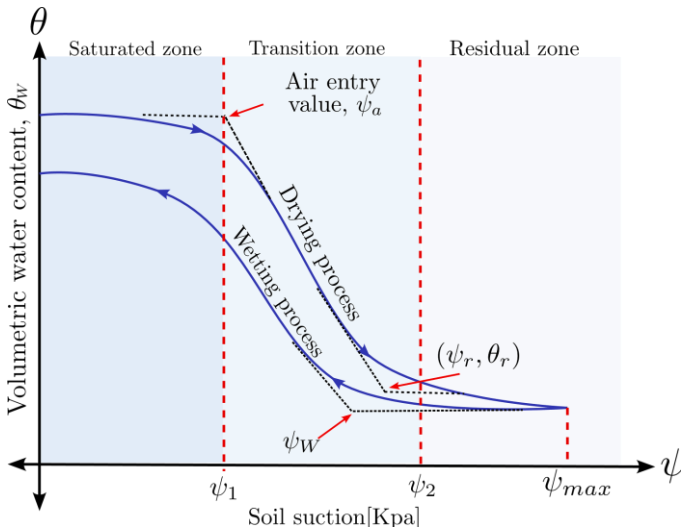

Figure 1. Volumetric water content as function of soil suction

Despite advances in experimental techniques such as pressure plate apparatus [10], tensiometers [11] and electrical conductivity sensors [12, 13], measuring the SWCC in the laboratory remains costly and time-consuming [14]. Consequently, numerous theoretical models have been proposed to simplify SWCC determination. These models often rely on empirical fitting parameters or mean-field approximations, which assume homogeneity and average out the complexities of pore-scale interactions [15-23]. While computationally efficient, such approximations fail to capture the intricate nonlinear and collective behaviors that occur at the pore scale.

Recognizing these limitations, pore network models have emerged as a more accurate representation of soil microstructure [24]. Traditional models for predicting unsaturated soil properties, such as the bundle-of-capillary-tubes model, simplify the pore structure by treating it as a collection of independent capillaries [25]. While these models offer computational simplicity, they overlook the critical influence of pore connectivity and structural heterogeneity on soil behavior.

Recent advancements in machine learning techniques have shown potential in overcoming these limitations by directly predicting the SWCC from experimental data without relying on oversimplified assumptions or mean-field approximations. These models can capture complex, non-linear relationships between suction, water content, and soil properties, providing a more accurate representation of the SWCC in unsaturated soils [26, 27]. However, despite their promising capabilities, machine learning models also face several limitations. They often require large and high-quality datasets for training, and the performance of the model is heavily dependent on the quality of the data.

In contrast, models that conceptualize soil as interconnected pore networks enable the simulation of water flow and hysteresis at the pore scale. These approaches are particularly valuable for estimating hydraulic conductivity, as they incorporate essential characteristics of the pore structure. However, despite these advances, many pore network models do not account in detail for hysteresis phenomena, which are critical in unsaturated soils due to the distinct behaviors observed during wetting and drying cycles [25].

Traditional pore network approaches often overlook the complex interactions among pores or rely on simplified assumptions, commonly represented by mean-field approximations. Such methods, akin to those used in statistical mechanics to simulate atomic and molecular systems—such as lattice gases [28] and neural networks [29]—have been extensively utilized [30–32]. However, the unique behavior of SWCC has sparked discussions regarding the adequacy of relying solely on approximations for porous systems. Furthermore, pressure gradients across distant boundaries within a soil sample during drainage may yield retention curves of greater complexity than those typically captured by theoretical models [33].

To address these limitations, Monte Carlo simulations offer a powerful alternative. By modeling individual pores and their interactions probabilistically, these simulations capture the stochastic and collective dynamics of pore networks, including hysteresis effects and phase transitions. Although Monte Carlo methods have been used to calibrate parameters for van Genuchten-type models [34], their direct application to simulate and analyze hysteresis in pore networks has been limited. This study aims to bridge this gap by integrating a pore network model with Monte Carlo simulations to explore the SWCC and its hysteretic behavior. Unlike mean-field approximations, this approach explicitly considers pore-to-pore interactions and their impact on macroscopic soil properties. By simulating wetting and drying processes in detail, it provides a robust framework for understanding and theoretically predicting unsaturated soil behavior.

Additionally, we investigated the collective interactions of pores under pressure using Monte Carlo simulations to model and analyze the soil drainage process. In this context, Monte Carlo techniques perform statistical analyses by substituting probability distributions for factors with inherent uncertainty [35]. By recalculating interactions thousands of times, these simulations generate detailed retention curves that reflect the complex dynamics of porous systems. Unlike previous treatments that relied on approximations [33], this method provides a more comprehensive representation of the pore-scale processes driving soil behavior.

The rest of this paper is structured as follows: Section 2 introduces the methodology; Section 3 explores hysteresis in the SWCC; Section 4 outlines the theoretical framework for pore interactions in soils; Section 5 describes the statistical model used to simulate the porous network; Section 6 explains the Monte Carlo simulation process; Section 7 presents numerical results, including the retention curves obtained; and Section 8 concludes with key findings and future directions.

2. Research Methodology

This study aimed to develop a theoretical model based on a pore network approach to simulate the SWCC and analyze hysteresis in unsaturated soils. The following methodological steps were undertaken (Figure 2):

- Review of Hysteresis in Unsaturated Soils: The initial phase involved an extensive review of the hysteresis phenomenon in unsaturated soils, focusing on the primary causes and characteristics affecting soil–water interactions. This review provided essential context for understanding how hysteresis arises in soils due to factors such as the "ink bottle" effect and variations in contact angles. These insights were critical for accurately modeling the behavior of the SWCC.
- Pore Network Simulation: Following the hysteresis review, the soil was modeled as a complex network of interconnected pores, approximating the soil structure as a lattice system. Each pore was represented as a node, with the channels between pores modeled as connections. The state of each pore, influenced by its neighboring pores, governed the flow behavior within the network.
- Application of the Ising Model: A two-dimensional Ising model was adapted to study the interactions among soil pores. Originally developed for ferromagnetic systems, this model was repurposed to simulate the tendency of pores with similar water saturation states to cluster together. In this approach, pores were represented in one of two states: filled or unfilled, corresponding to water retention or expulsion, respectively. Additionally, an external pressure field was incorporated into the model to simulate the effects of soil suction on the pore network.
- Monte Carlo Simulation: Monte Carlo simulations were employed to explore water flow behavior in porous media under varying pressure conditions. A probability distribution was utilized to simulate multiple configurations of the pore network, effectively capturing the nonlinearity and hysteretic nature of the SWCC. Thousands of pore interactions were recalculated, enabling the statistical analysis of variables such as pore filling states, mean energy, and phase transitions.
- Hysteresis Analysis: The hysteresis behavior in the soil–water characteristic curve (SWCC) was analyzed by simulating wetting and drying cycles within the pore network. Changes in water content and suction over time were observed, and the network's filling states were evaluated during each cycle, successfully reproducing the characteristic hysteretic loop of the SWCC.

3. Hysteresis in the Soil–Water Characteristic Curve

This section describes the theoretical derivation of hysteretic behavior in the SWCC. Soils retain more water at a given tension during desorption than during absorption [36]. This history-dependent behavior, analogous to similar physical processes, is known as hysteresis. Hysteresis in the soil suction–water content relationship, observed when soils are cyclically wetted and dried, refers to the nonunique relationship between the pressure head and the water content in the SWCC [37].

During infiltration, as the water content increases, the pressure head also increases. Therefore, the SWCC can be described by a unique function. However, when the input direction reverses during drainage, the pressure head and water content (ψ, θ) do not follow the original path, requiring a different but still unique function to describe the SWCC.

Analyses of hysteresis typically adopt one of three approaches: 1) Theoretical models. 2) Experimental–analytical models. 3) Numerical simulations.

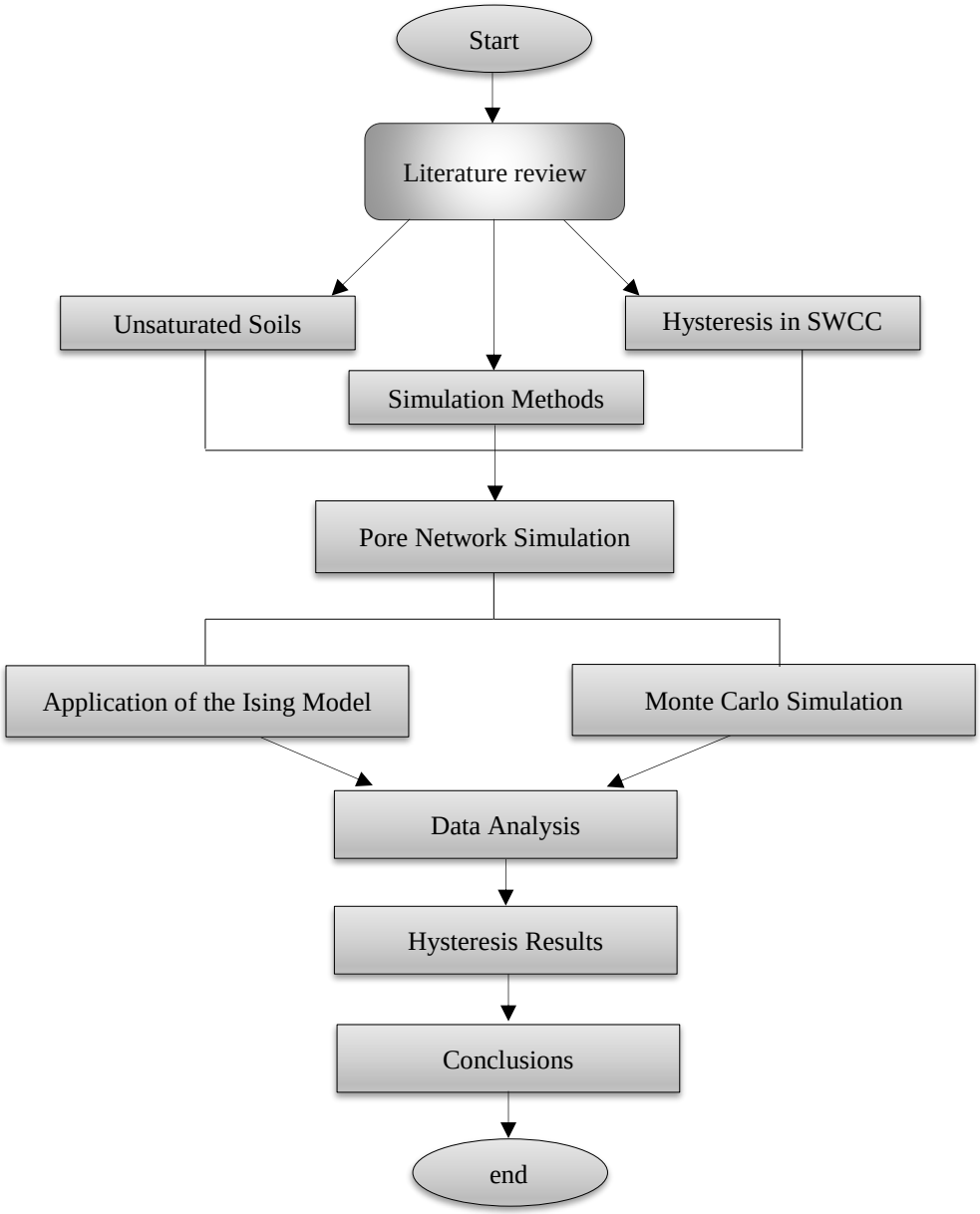

Figure 2. Research flowchart

3.1. Theoretical Models

Theoretical models for describing the retention behavior of soils are typically divided into independent [38-40] and dependent pore models [33, 41, 42]. These classifications depend on whether pore drainage is assumed to be independent of or influenced by the state of neighboring pores. In both types of models, the soil matrix is divided into pore domains characterized by:

- Wetting pore radii: Control water filling.
- Drying pore radii: Control water emptying.

3.2. Experimental–Analytical Models

Experimental–analytical models often scale the primary, secondary, and higher-order scanning curves from the main hysteresis curve [43–46]. These models use various analytical expressions to describe the SWCC. Commonly applied models include: Brooks–Corey, Farrell–Larson, Fredlund–Xing, Gardner, McKee–Bumb, Kosugi, van Genuchten, Campbell, Russo, Tani, Omuto, and Dexter models [2, 21, 22]. These models allow the determination of shape parameters, referred to as hydraulic parameters, by fitting experimental data to water-retention functions. However, the

methods for measuring soil hydraulic parameters are often time-consuming and expensive. Generating datasets suitable for calibrating analytical models may take several months [37]. To address this challenge, transient experiments involving hysteresis have been proposed, where data are analyzed using computational tools to obtain information about soil hydraulic properties [47]. Other methods leverage experimental techniques like X-ray microtomography and numerical simulations to examine the internal liquid distribution in soil pores [48–50]. However, numerical simulations are typically limited to relatively small numbers of pores in the soil matrix.

3.3. Theoretical and Computational Framework

In this work, a theoretical and computational framework was explored to address these limitations. This framework considers the collective interactions of pores in unsaturated soils. Without relying on parametric fitting or analytical approximations, the behavior of the main SWCC curves was derived. For this analysis, the soil system was conceptualized as a solid frame divided into pore domains characterized by their filling states. The bulk domain behavior was studied using concepts derived from magnetic materials. In these systems, small groups of atoms (where all electrons share the same magnetic orientation) are analyzed. One of the simplest and most important statistical physics models for studying domain formation in magnetic systems is the Ising model. In the absence of external forces, the Ising model provides an analytical solution. However, under the influence of external fields, a numerical solution is required. In this study, the collective interactions of pores in unsaturated soils were examined under external pressures, and their effects on the SWCC were analyzed using the Ising statistical model. This model, initially developed to predict hysteresis in the magnetization of magnetic materials, was adapted to study the hysteresis phenomenon in soil systems. The main characteristics of the Ising model and the numerical methodology used to approach this problem are described in the next section.

4. Model of Porous Systems

In this study, we propose a theoretical model to describe the hysteresis behavior observed in the SWCC of unsaturated soils. The model is constructed using a pore network approach, representing the soil as a lattice of interconnected pores. This representation enables effective simulation of fluid dynamics and hysteresis effects in unsaturated soils, which are fundamental for understanding the interaction between soil and water under varying pressure conditions.

The decision to model soil as a network of pores is based on the premise that the soil's hydraulic properties, particularly its water retention and flow behavior, are primarily governed by the geometry and connectivity of the pores. In reality, soils consist of large voids (pore bodies) and smaller, narrower sections (pore throats) that regulate fluid movement between these voids. By modeling these elements as a network, we aim to capture the complex flow behavior and hysteresis phenomena that occur when soils undergo cycles of wetting and drying [51]. Traditional models often emphasize macroscopic properties, such as porosity or permeability, but fail to account for the finer-scale behavior arising from pore connectivity and the dynamics of water movement at the pore scale. By representing soil as a network of interconnected pores, our model simulates and examines the underlying processes responsible for the characteristic hysteresis in the SWCC. This approach captures the intricate interplay of capillary forces, surface tension, and pore connectivity, which dictate how water enters and exits the soil during wetting and drying cycles.

Furthermore, the pore network model provides a flexible framework that can be tailored to various soil types and conditions by adjusting the parameters of the pore network.

4.1. Assumptions for Pore Network Modeling

To simplify the complex behavior of unsaturated soils and ensure computational feasibility, several assumptions were made in constructing the pore network model. These assumptions include:

- Two-Dimensional Pore Network: The pore structure is represented as a two-dimensional lattice. While this simplification does not fully capture the three-dimensional complexity of soil, it allows for efficient computation and is considered sufficient for modeling the primary hydraulic and hysteretic behaviors. This framework effectively incorporates variations in pore connectivity and accounts for the influence of local heterogeneities within the soil matrix.
- Binary Pore State: Each pore in the network is modeled with only two possible states: filled with water ($\sigma = 1$) or filled with air ($\sigma = -1$). This binary representation is effective for describing the fundamental hysteretic behavior of soils during wetting and drying cycles, where pores transition between retaining water and expelling air.
- Pore Connectivity and Aggregation: Pores are interconnected by "tunnels," and those sharing the same filling state (either filled with water or air) tend to form domains or clusters. This assumption enables the model to simulate the collective behavior of the pore network and observe cluster formation, which significantly contributes to the hysteresis observed in the soil–water characteristic curve (SWCC).

- External Pressure as an External Field: The model incorporates an external pressure field to simulate the effects of suction and pressure on the pore network. This external pressure influences the state of individual pores and, consequently, the overall soil–water characteristics. The approach is analogous to the influence of an external magnetic field in ferromagnetic systems, where the field drives state transitions within the system.

4.2. Model

This section presents the details of the model developed to describe the hysteresis observed in the SWCC for unsaturated soils. The model incorporates the effect of external pressure on the SWCC and is based on the assumption that the soil can be represented as a network of interconnected pores, as discussed in Section 4.1. This representation enables the investigation of energy changes associated with transitions between wet and dry states of the soil and their contribution to hysteresis.

First, a soil element of volume V was considered (Figure 3). The total volume of the sample can be expressed as: $V = V_s + V_v$, where V_s represents the solid volume and V_v, the void space. For simplicity, the void space is modeled as a set of interconnected pores on a two-dimensional lattice. Additionally, it is assumed that these pores can only be filled with water or air; therefore, the void volume consists of contributions from these two components: $V_v = V_w + V_a$.

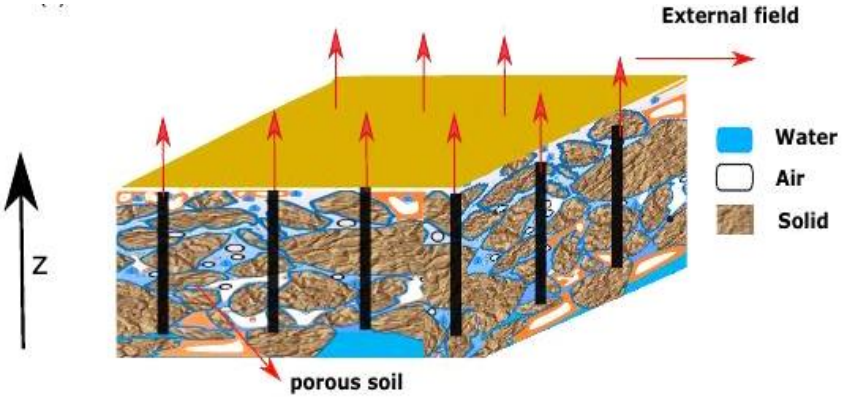

Figure 3. Illustration of soil with a qualitative depiction of its porous structure. An external field is applied in the +z direction (perpendicular to the plane). The soil is represented as a composite system consisting of solid material, air, and water

The aim of the model is to determine the energy required for a pore to transition between filled and empty states (or vice versa). Furthermore, the coordination number was examined, considering that each pore is connected to its neighbors through "tunnels," and pores with the same filling state tend to form clusters (domain formation). To calculate the change in a pore's state, the influence of external pressures in the soil system must be considered. This external influence is incorporated as a field affecting the entire network, analogous to an external magnetic field in a magnetic system (arrows in Figure 3).

For a pore at site i in the lattice, initially filled with water, the energy required to empty it ΔE_i is given by:

$$\Delta E_i = \Delta E_{wa} + \Delta E_s + W_{wa}, \quad (1)$$

where ΔE_{wa} represents the change in surface energy, which quantifies the disruption of intermolecular bonds when a surface is created or destroyed. The surface energy of a pore strongly depends on the filling of all N connected neighboring pores with index j.

If the pore transitions from $\sigma_i = 1 \rightarrow -1$ while a neighboring pore is in the state $\sigma_j = -1$, a surface disappears, and the corresponding energy per unit area is γ_{wa_j} (see Figures 4-a and 4-b). This leads to:

$$\Delta E_{wa_j} = -\gamma_{wa_j}, \quad (2)$$

and when considering all neighboring pores,

$$\Delta E_{wa} = \sum_{j=1}^{N} \pm \gamma_{wa_j} a_{t,j}, \quad (3)$$

where γ_{wa_j} is the surface energy between pore pairs, and $a_{t,j}$ the area of the tunnels connecting pore i to its N closest neighbors, each with area $a_{t,j}$. The transitions in pore states (σ_i) are influenced by the states of neighboring pores (σ_j), allowing the model to dynamically capture local variations in connectivity and their effects on the overall structure of the pore network.

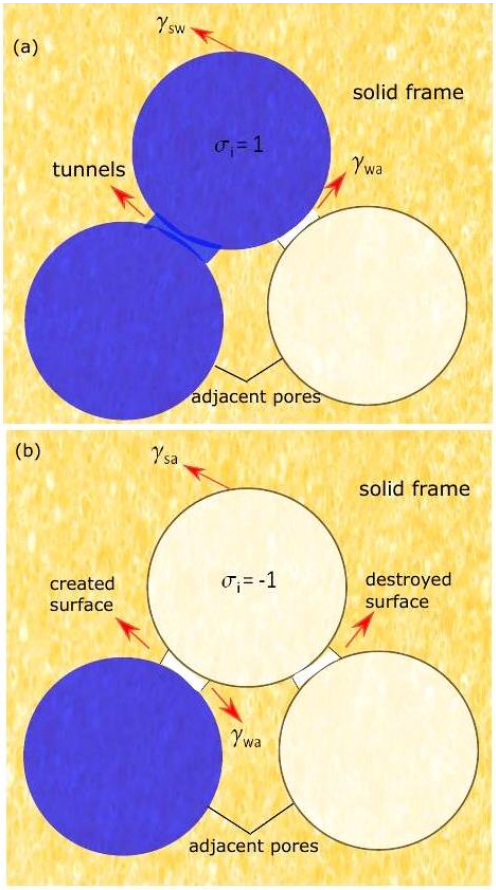

Figure 4. Schematic representation of identical porous assembly elements. (a) A single pore i initially filled with water ($\sigma_i = 1$) interacting with the external soil frame (γ_{sw}) and neighboring empty pores (γ_{wa}). (b) Illustration of the surface changes due to the emptying of the pore $i(\sigma_i = -1)$, showing the destruction of the filled surface and creation of an empty surface as the pore transition to its dry state.

The term ΔE_s represents the change in surface energy at the solid–water and solid–air interfaces. For instance, when pore i is filled with water ($\sigma_i = 1$) and surrounded by solid material, the destruction of the solid–water interface during emptying results in a change of energy in the boundary interface from γ_{sw} to γ_{sa} (see Figures 4-a and 4-b). Thus:

$$\Delta E_s = (\gamma_{sa} - \gamma_{sw})A_p, \tag{4}$$

where A_p is the solid interface area of the pore.

Finally, the term W_{wa} in Equation 1 accounts for the volume work associated with the pressure change (ψ_{ext}) in pore i of volume V_v during emptying. Therefore, if the pore state transitions from $\sigma_i = 1 \rightarrow -1$, the corresponding energy difference is:

$$W_{wa} = \psi_{ext} V_p. \tag{5}$$

A similar argument applies during filling ($\sigma_i = -1 \rightarrow \sigma_i = 1$), with the signs in Equations 2, 4 and 5 reversed. In the following section, the physical model and its main implications are used to demonstrate how this theory predicts the hysteresis behavior in the SWCC.

5. Ising Model in Porous Systems

The physical model used in this study to reproduce the characteristic hysteresis curves associated with the hydraulic and mechanical processes in unsaturated soils was adapted from the Ising model [35], originally developed to describe ferromagnetic systems. This section details the rationale behind this adaptation, the specific implementation of the model, and its key limitations.

The Ising model, a fundamental tool in statistical physics, was first introduced by Lenz in 1920 to describe magnetic domain formation in ferromagnetic materials [52]. It provides a robust conceptual framework for understanding phase transitions in systems composed of individual elements (e.g., spins) that interact with their nearest neighbors. This

framework closely aligns with the behavior of soil pore systems, where each pore (or grid cell) can exist in one of two states (e.g., saturated or unsaturated), and interactions between neighboring pores significantly influence the system's overall dynamics.

Similar to how spins in the Ising model align to minimize system energy [53], neighboring pores in soil systems exhibit a tendency to aggregate into organized spatial patterns, particularly under critical conditions. These characteristics make the Ising model an effective choice for representing the dynamics of pore-filling behavior [33].

To adapt the Ising model for soil systems, the pore network was represented as a bidimensional lattice where each site i on layer k was assigned an Ising variable $\sigma_i(\sigma_i = 1)$ to indicate its filling state (saturated or unsaturated). The total energy of the system, or Hamiltonian, was derived under the following assumptions:

- Nearest-Neighbor Interactions: Pores interact primarily with their immediate neighbors within the same soil layer. These interactions represent local processes, such as water redistribution.
- Tendency for Aggregation: To reflect the natural clustering tendency of pores with similar filling states, "ferromagnetic" interactions were included within the lattice. These interactions mimic the energy minimization observed in spin alignment in ferromagnetic systems.

The Hamiltonian, formulated in terms of intralayer coupling, quantitatively describes the energy dynamics within the system by capturing interactions between neighboring pores. The dimensionless Hamiltonian describing these intralayer interactions is expressed as:

$$H(\sigma_i) = -\beta \sum_{\langle i,j \rangle} J_j \sigma_i \sigma_j - \beta \psi' \sum_i \sigma_i, \quad (6)$$

where the β factor in Equation 6 represents the reciprocal of the thermodynamic temperature for systems with thermal interactions. Because energy transfer in the form of heat was not considered in this work, a statistical interpretation of β was used. In this framework, a large ensemble of copies of a porous sample is considered, with each copy having a distinct distribution of filling states. Copies with the same energy form a microstate. In this context, β is a property of the system that defines the variation in the number of accessible states as a function of energy. Here, the number of accessible states represents the diverse and complex combinations of pores with a given filling state. Additionally, β preserves certain conditions that define the system at a macroscopic level. For example, if β increases, the system tends to adopt more ordered configurations, indicating lower energy.

The term J_j in Equation 6 is the interaction energy between pore *i* and its neighboring pore *j* in the lattice. This interaction is derived as:

$$J_j = \frac{\gamma_{wa_j} a_{t,j}}{2}. \quad (7)$$

Additionally, the pore state of a neighboring site *j* is characterized by $\sigma_j = \pm 1$, indicating whether it is saturated or unsaturated.

To account for external mechanical forces, an additional term ψ' was introduced in the Hamiltonian, analogous to an external magnetic field in the Ising model. This term simulates the effects of soil pressure and is expressed as:

$$\psi' = \frac{\Delta E_s - \psi_{ext} V_p}{2}. \quad (8)$$

The introduction of an external field to simulate soil pressure effects in the model accounts for the influence of external mechanical forces on pore states, akin to the role of an external magnetic field in the Ising model. While the specific formulation of the external field in this model is novel, it is grounded in established physical principles and aligns with prior theoretical frameworks in unsaturated soil mechanics. In these frameworks, external stresses are known to modify soil water retention behavior by altering pore connectivity and geometry [54].

Although direct experimental studies on the exact implementation of the external field are not available, the modeled behavior qualitatively aligns with observed soil responses in experimental studies [55]. For instance, SWCC under varying mechanical stresses exhibits trends consistent with the model, such as shifts in saturation thresholds with increased pressure. Additionally, the hysteresis captured by the external field closely mirrors experimentally observed hysteresis in soil-water retention caused by changes in effective stress.

Considering these interactions, the total interaction energy $J = \sum_{j=1}^{N} J_j$, external pressure ψ', and the factor β are regarded as the primary control parameters of the system. Depending on the values of these parameters, the system may exhibit ordered or disordered states, as well as intermediate critical states.

6. Monte Carlo Simulation

One of the main properties of the Ising model is its ability to calculate phase transitions in the system of interest. During a phase transition, certain properties change, often discontinuously, due to changes in external conditions such as temperature or pressure.

To examine the emergent phases of the Ising model, a Monte Carlo simulation was performed under fixed boundary conditions in a porous lattice subjected to external pressure. Conceptually, this simulation can be viewed as a random walk through the state space of the system. To ensure reliable results, averages of the variables of interest were calculated over a large number of iterations. The Monte Carlo method was implemented in C++, which allowed for accurate modeling of stochastic processes by generating the necessary random numbers.

At the start of the simulation, the porous system was initialized with all pores completely filled with liquid. While deterministic, this initial configuration provided a consistent baseline for analysis. The algorithm randomly selected pores and attempted to change their states based on energy considerations governed by the transition rates defined in Equation 9. Transitions that reduced the system's energy ($\Delta E_i \leq 0$) were accepted, while others were rejected. This process was repeated iteratively until the system reached equilibrium, defined as the convergence of running averages for the energy per pore ($\langle E \rangle$) and the filling states ($\langle \sigma \rangle$) within a small tolerance.

$$\begin{aligned} Rate[\sigma_i = 1 \rightarrow \sigma_i = -1] \quad &= \Gamma, \quad \text{if } \Delta E_i \leq 0 \\ &= 0, \quad otherwise \end{aligned} \tag{9}$$

6.1. Simulation Robustness and Sensitivity Analysis

To ensure the robustness of the results, multiple iterations of the Monte Carlo simulation were conducted. Across different runs, the system consistently demonstrated reliable convergence of averages, confirming stability under the given conditions. While minor statistical variations in the critical point ($1/\beta$) were observed due to the inherent randomness of the method, these deviations were negligible and did not affect overall trends. Specifically, the behavior of critical points, such as their shift with increasing external pressure (ψ'), was reproducible across simulations, further validating the model.

A sensitivity analysis was conducted by varying the lattice size (N) and the number of Monte Carlo steps (NMC). Larger lattices and longer simulation times produced smoother fluctuations and more precise estimates of critical points. However, the fundamental behaviors—such as phase transitions and hysteresis phenomena—remained consistent, confirming that the results reflect the system's intrinsic dynamics rather than artifacts of simulation parameters.

6.2. Exploring Hysteresis Behavior

After the system reached equilibrium, average energy and pore filling states were obtained. To explore phase transitions, the hysteresis behavior in the SWCC was reproduced using the following procedure:

- Initialization: Start with a sufficiently large negative external pressure ψ' so that all pores are in the filled state $\sigma = 1$.
- Pressure Increase: Slowly increase the applied pressure. At a certain value of ψ', the local pressure at specific pores will become positive, causing those pores to change state.
- Cascading Effect: The change in state alters the effective pressure of neighboring pores, potentially causing them to transition as well. This cascading effect was observed until the system stabilized.
- Stable State Measurement: After stabilization, the total average filling state $\langle \sigma \rangle$ was recorded.
- Incremental Pressure: Increment the applied pressure slightly and repeat the process until all pores transitioned to the same state. This procedure generated the lower half of the hysteresis loop $\langle \sigma_u \rangle$.
- Reversing Pressure: The upper half of the hysteresis loop was obtained by reversing the procedure—decreasing the external pressure ψ'. The symmetry between the upper and lower halves of the loop $\langle \sigma_l \rangle$ is expressed as:

$$\langle \sigma_u \rangle(\psi') = -\langle \sigma_l \rangle(-\psi'). \tag{10}$$

6.3. Key Features of the Dynamics

- State Transitions: If the system starts in a stable configuration and the external pressure increases while allowing the system to relax, no pore changes its state more than once.
- Final Configuration Stability: The final stable configuration remains consistent regardless of the order in which unstable pores transition.
- Symmetry in Hysteresis: The symmetry in the hysteresis loop reflects the system's inherent energy dynamics under varying external pressures, as observed in experimental studies.

This method reliably reproduced the characteristic hysteresis loops associated with the SWCC, demonstrating how external pressure influences the dynamic interactions within the pore network.

7. Results

The simulation algorithm constructs a random two-dimensional lattice with $N \times N$ sites (representing the pores), such that each site has exactly four neighbors (Figure 5). The precise algorithm involves labeling each site (each pore) with a pair of indices (i, j). Each site (i, j) is connected to its neighbors $(i, j+1), (i, j-1), (i+1, j), (i-1, j)$ for all sites. Periodic boundary conditions are applied. In this simulation, $N = 10^2$ and $NMC = 10^4$ Monte Carlo steps were used.

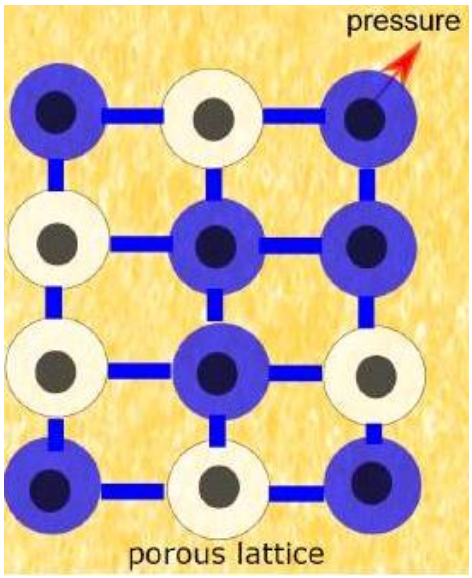

Figure 5. Top view of a porous lattice structure representing a section of soil. The white spheres denote empty pores, while the blue spheres represent filled pores. The rectangular connections between the pores depict tunnels facilitating fluid movement. The red arrow indicates the applied external pressure direction.

To analyze the system's critical behavior, specific order parameters were calculated. An order parameter measures the degree of order across boundaries in a phase-transition system. Two order parameters were considered: the average energy of interactions per pore ⟨E⟩ and the filling states for all pores ⟨σ⟩.

In Figure 6-a, the results of $\langle E \rangle$ are presented as a function of the inverse β factor for three values of external pressure ψ': 0,0.3,0.5. The behavior of $\langle E \rangle$ reflects the soil system's energy state as it transitions between saturated (water-filled pores) and unsaturated (air-filled pores) phases. Critical transition points, marked by changes in the slope of the curves, correspond to the energy required to shift the system from one phase to another. At zero external pressure, the system transitions between phases at a relatively low $1/\beta$, meaning less energy is required for phase transitions. This behavior mimics soils in environments without external stress (e.g., free drainage), where phase changes occur more readily. As external pressure increases, critical points shift to higher $1/\beta$, indicating that more energy is needed for phase transitions. This behavior resembles unsaturated soils under mechanical stress or capillary tension, where external forces stabilize the water-filled state and resist drainage. The observed energy shift with increasing external pressure (ψ') directly correlates with the concept of matric suction in unsaturated soils. Higher suction forces energetically favor water-filled pores, delaying transitions to air-filled states. This reflects the influence of capillary forces in unsaturated soils, where water retention increases under tension.

The dependency on $1/\beta$ illustrates how macrostate transitions depend on the diversity of accessible microstates and the overall ordering of pore configurations. Here, β does not represent thermodynamic temperature but instead characterizes the system's variation in accessible states as a function of energy.

At lower $1/\beta$ (higher β), the system tends toward ordered configurations with lower energy states, corresponding to stable pore filling states that minimize system energy. Conversely, at higher $1/\beta$ (lower β), greater variability in microstates allows access to higher-energy configurations, leading to phase transitions.

This framework relates to the complexity and heterogeneity of unsaturated soils. A higher β suggests the system stabilizes in specific configurations (e.g., water-filled or air-filled pores), resembling soils under strong retention forces. A lower β implies more disorder, allowing phase transitions as the system explores a wider range of states. This highlights the interplay between pore filling states and the energy landscape, where β modulates the balance between order and configurational diversity.

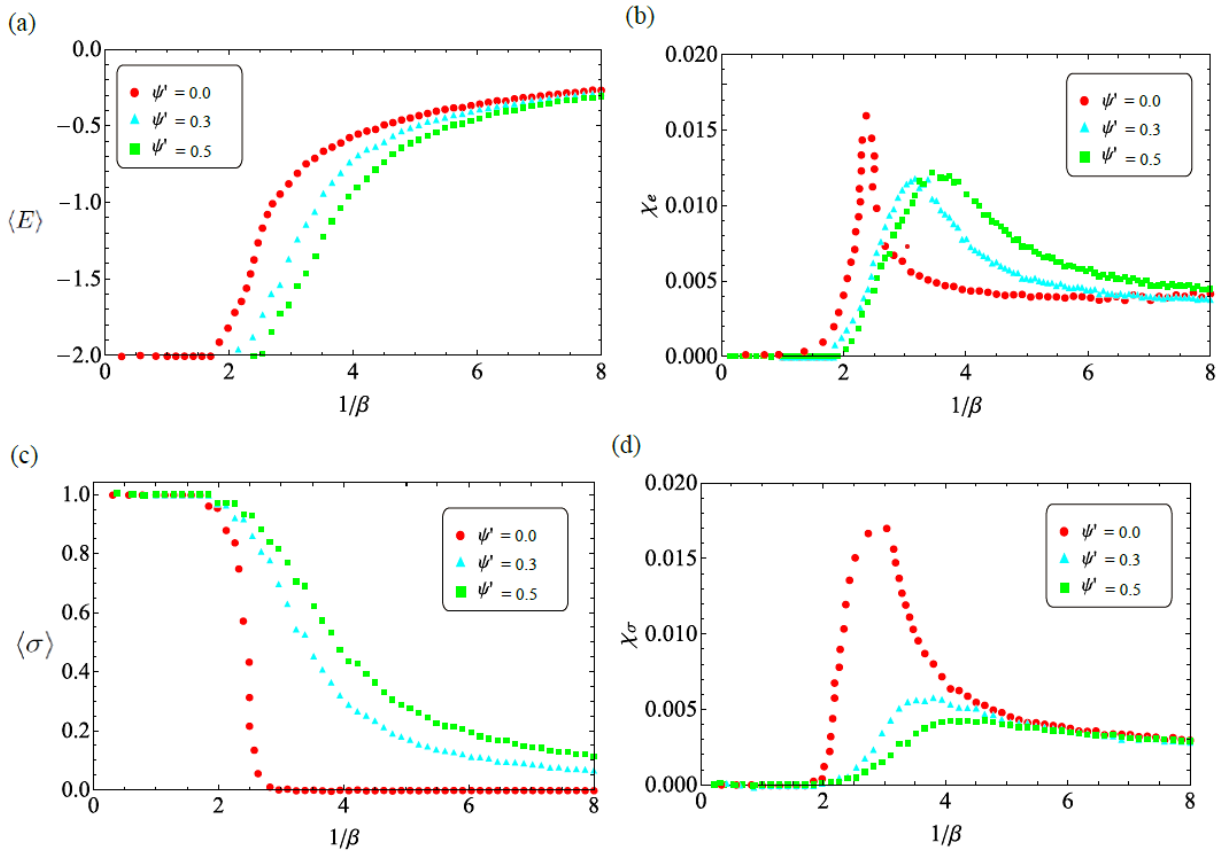

Figure 6. Order parameters (a) $\langle E \rangle$ and (c) $\langle \sigma \rangle$, along with their fluctuations in (b) χ_e and (d) χ_σ. The peaks in (b) and (d) indicate the $1/\beta$ values corresponding to phase transitions in mean energy and pore filling states, contingent on the applied external pressure.

In Figure 6-c, $\langle \sigma \rangle$ is plotted as a function of $1/\beta$. When $\psi' = 0$, the system fluctuates between positive (water-filled pores) and negative (air-filled pores) states, depending on $1/\beta$ value.

With increasing ψ', the curves shift rightward, indicating that external pressure biases the system toward water-filled pores, making phase transitions more energetically difficult. This aligns with the interpretation of external pressure stabilizing certain configurations. At higher ψ', the system resists transitioning to air-filled states due to the additional energy barrier imposed by external forces.

The rightward shift in curves can also be understood through the system's energy landscape. With $\psi' = 0$, the energy barrier for state transitions is symmetric, allowing frequent fluctuations between water-filled and air-filled pores. However, with $\psi' > 0$, the landscape becomes asymmetric, favoring water-filled configurations. This explains why larger $1/\beta$ (lower β) values are required to overcome the bias imposed by external pressure.

The point at which the system transitions sharply from one state to another (e.g., from $\langle \sigma \rangle = 1$ to $\langle \sigma \rangle = 0$) represents the critical point of the phase transition. For ψ=0, this critical point occurs at a lower $1/\beta$, indicating lower energy requirements for the transition. When $\psi' > 0$, the critical point shifts to a higher $1/\beta$, reflecting an increase in the energetic threshold required for the transition due to external pressure.

The fluctuation dynamics for E and σ are presented in Figures 6-b and 6-d, respectively, to provide a detailed analysis of the system's behavior near the critical points. These graphs offer significant insights into the energetic and configurational instabilities characteristic of phase transitions.

Figure 6-b depicts the fluctuations in the energy per pore (χ_E) as a function of $1/\beta$. The maxima of these fluctuations correspond to the critical points, where the system's energy landscape exhibits heightened instability, facilitating frequent transitions between metastable and equilibrium states. With increasing external pressure ψ', these peaks in χ_E shift to higher values of $1/\beta$, signifying an elevated energetic threshold required to trigger phase transitions. Moreover, the observed reduction in peak intensity at higher ψ' indicates that external pressure acts as a stabilizing factor, attenuating energy fluctuations and thereby promoting a more ordered and stable configuration within the pore network.

Similarly, Figure 6-d illustrates the fluctuations in pore filling states (χ_σ), which also exhibit sharp peaks near the critical points. These peaks signify rapid transitions between water-filled and air-filled configurations, reflecting the system's instability during phase transitions. Consistent with χ_E in Figure 6-b, the peaks in χ_σ shift to higher $1/\beta$ as ψ'

increases, aligning with the observation in Figure 6-c that external pressure raises the energy barrier required for phase transitions. At higher ψ', the system undergoes fewer state changes, indicating increased stability and a pronounced preference for water-filled configurations due to the biasing effect of external pressure.

The nonequilibrium response of the Ising lattice at constant energy $(1/\beta)$, or equivalently, the saturation-varying pressure ψ' (SWCC curve) is investigated in Figure 7.

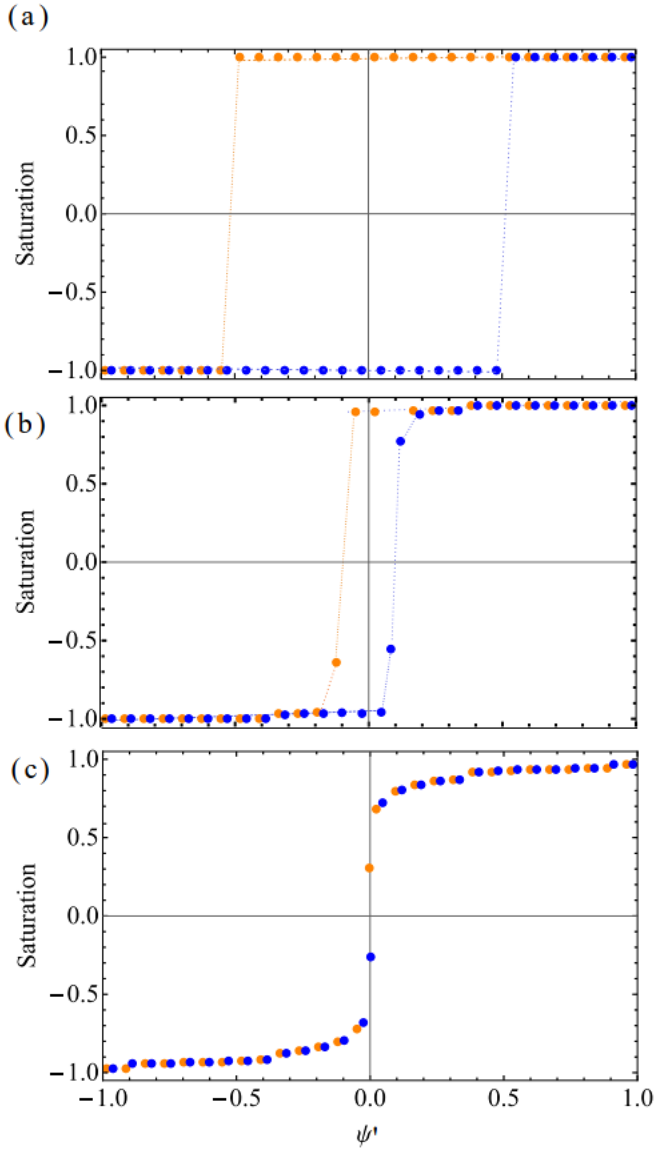

Figure 7. Plots showing the saturation as a function of external pressure ψ', for different $1/\beta$ values. Panels correspond to (a) $1/\beta = 1.5$, (b) $1/\beta = 1.9$, and (c) $1/\beta = 2.5$. Notice the hysteresis loop formed by changing the external pressure from −1 to 1. The orange points represent the initial direction, while the blue points correspond to the reversed direction.

In Figure 7-a, the hysteresis loop exhibits a pronounced rectangular shape, indicating strong metastability during the saturation process. In this state, the system takes distinctly different paths for pore filling and emptying under varying external pressure (ψ'). This behavior is characteristic of first-order phase transitions, where metastable states dominate and significant energy is required to transition to equilibrium. The wide area of the loop reflects the high energy barrier between water-filled and air-filled states, a feature typical of systems operating at low energy or high disorder.

As shown in Figure 7-b, the area of the hysteresis loop decreases compared to Figure 7-a. With increasing energy, the system exhibits reduced metastability, and the paths for filling and emptying become more similar. This behavior suggests that the energy barriers between states are smaller, allowing the system to transition more easily between water-filled and air-filled configurations. The reduction in loop area is consistent with the expected behavior of porous systems as they approach equilibrium at higher energy levels, where disorder is lower and transitions are less constrained.

Finally, in Figure 7-c, the hysteresis loop disappears entirely, indicating that the system transitions smoothly between states without path-dependent behavior. This suggests that the system has reached a state where it is no longer metastable, and the filling and emptying processes have become fully reversible. This marks the progression from a

strongly metastable regime to one of equilibrium, highlighting the diminishing influence of energy barriers as the system approaches higher energy levels.

This disappearance of hysteresis marks the transition from a first-order to a second-order-like phase transition, where the system equilibrates without energetic barriers.

To further understand the behavior of the statistical quantities, Figures 8-a to 8-c present the spatial patterns of the pores in the lattice corresponding to equilibrium microstates with $1/\beta = 2.5$. At a pressure of $\psi' = -0.48$, the system predominantly exhibits water-filled pores, representing a saturated state. This condition reflects the scenario where the external pressure matches the pressure of the soil material, thereby stabilizing the water-filled configuration. In contrast, when $\psi' = 0.48$ becomes positive, the pores are primarily air-filled, mimicking a drainage process. These configurations correspond to the left and right sides of the hysteresis loop, respectively, as shown in Figure 7. This demonstrates how external pressure biases the system toward specific configurations, directly impacting the shape and area of the hysteresis loops.

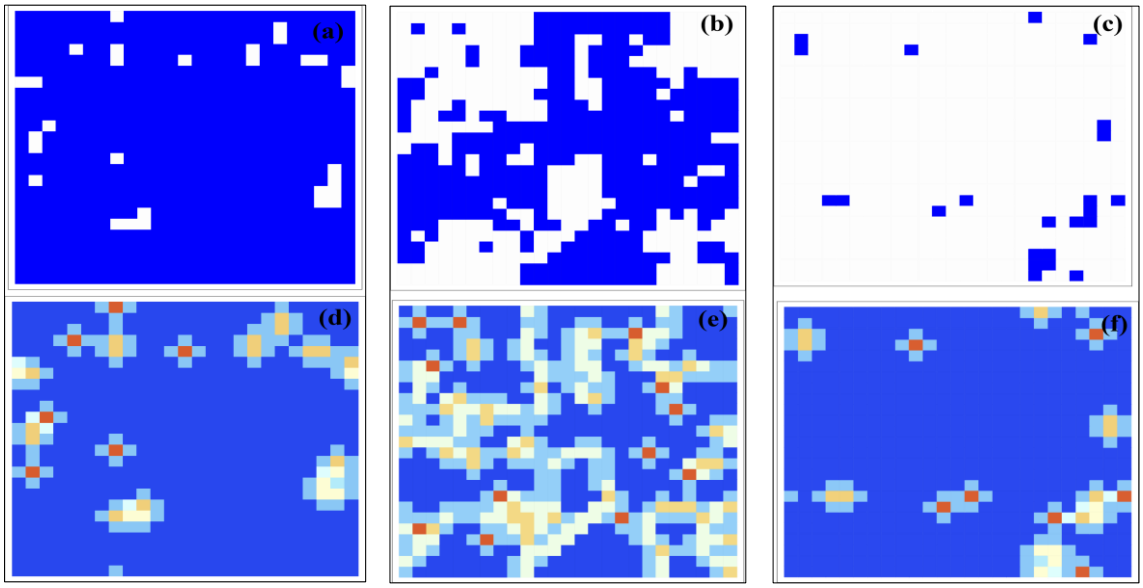

Figure 8. Three random microstates of a $10^2 \times 10^2$ porous lattice with periodic boundary conditions, corresponding to an equilibrium macrostate with $1/\beta = 2.5$ under varying external pressure. Subfigures (a), (b) and (c) illustrate the system configurations at external pressures $\psi' = -0.48$. (b) $\psi' = 0$. (c) $\psi' = 0.48$, respectively. The energy per pore for these configurations is shown in subfigures (d), (e), and (f) as (d) $\psi' = -0.48$, (e) $\psi' = 0$, and (f) $\psi' = 0.48$, respectively. These configurations and energy distributions highlight the interplay between the system's energetic landscape and configurational dynamics, emphasizing their roles in determining the stability and transitions of the porous structure.

Additional insight into the system's behavior is provided in Figures 8-d to 8-f, which display the energy per pore for a microstate with $1/\beta = 2.5$ under different external pressure values. These spatial patterns intuitively illustrate how saturation (Figure 6), χ_E, χ_σ (Figures 6-b and 6-d) evolve with changes in energy $(1/\beta)$. At the critical point, a bifurcation occurs, leading to two equally probable equilibrium macrostates, corresponding to positive (1) or negative (-1) saturation. The system alternates between these two states, which explains the sharp peaks observed in χ_E and χ_σ at the critical point.

These spatial patterns establish a clear connection between microstates, energy, and the transitions observed in the hysteresis loops. They highlight how external pressure modulates both the system's energetic landscape and its configurational dynamics, emphasizing its role in determining the stability and transitions of the porous structure.

8. Conclusions

This study introduces a novel approach to modeling the soil–water characteristic curve (SWCC) in unsaturated soils, providing a robust theoretical and numerical framework for estimating soil properties. By adapting the Ising model, traditionally used for ferromagnetic systems, this research effectively represents pore interactions and phase transitions in soils, shedding light on the aggregation tendencies of similarly filled pores. The incorporation of an external field to simulate soil pressure effects highlights the influence of external forces on pore filling states, moisture retention, and the SWCC.

Key findings from Monte Carlo simulations reveal the critical role of external pressure in stabilizing water within pores, delaying drainage, and increasing the energy barrier for phase transitions. These results align with physical

observations of capillary and suction effects that govern the retention and release of water in unsaturated soils under varying pressures and temperatures. Fluctuations in pore filling states (χ_σ) capture the configurational dynamics, while energy fluctuations (χ_E) highlight the system's energetic instability at critical points. The observed shift in critical points and suppression of fluctuations with increasing external pressure (ψ') demonstrate how external forces promote more stable and ordered states, delaying phase transitions.

Additionally, the term ΔE_S was shown to counteract external pressure effects, stabilizing water-filled pores, whereas increased external pressure facilitates pore drainage as ψ' approaches zero.

The model successfully captures hysteresis in the SWCC, which arises from global soil pressure effects. This hysteresis is critical for understanding soil–water retention dynamics and is attributed to phase transitions between metastable and equilibrium states, requiring specific energy thresholds dependent on soil pressure. These findings emphasize that energy input is fundamental to phase transitions, with significant implications for soil moisture retention under varying external forces.

Despite its success, the Ising model has some limitations. Specifically, it does not account for variations in pore size, and it assumes only two pore states (fully filled or empty). To enhance the model's realism, future work could focus on incorporating partially filled pores, which would better represent the intermediate states often observed in real soil systems. Experimental validation will also be essential to confirm the model's applicability and refine its predictive capabilities. Despite the absence of experimental applications at this stage, this research establishes a strong theoretical foundation and opens new pathways for understanding soil behavior under varying moisture conditions. These advancements hold great potential for practical applications in soil science and engineering.

9. Declarations

9.1. Data Availability Statement

The data presented in this study are available in the article.

9.2. Funding and Acknowledgements

The author gratefully acknowledges the financial support provided by Universidad Mariana and would like to thank Prof. Juan Carlos Salazar for his valuable insights and engaging discussions, which greatly contributed to this work.

9.3. Conflicts of Interest

The author declares no conflict of interest.

10. References

[1] Fredlund, D. G. (1995). The scope of unsaturated soil problems. Proceedings of the First International Conference on Unsaturated Soils, UNSAT'95, 6-8 September, Paris, France.

[2] Rahardjo, H., Kim, Y., & Satyanaga, A. (2019). Role of unsaturated soil mechanics in geotechnical engineering. International Journal of Geo-Engineering, 10(1), 1–23. doi:10.1186/s40703-019-0104-8.

[3] Vanapalli, S. K., Fredlund, D. G., Pufahl, D. E., & Clifton, A. W. (1996). Model for the prediction of shear strength with respect to soil suction. Canadian Geotechnical Journal, 33(3), 379–392. doi:10.1139/t96-060.

[4] Zhu, S., Zhang, L., & Wu, L. (2024). Simulation of hydro-deformation coupling problem in unsaturated porous media using exponential SWCC and hybrid improved iteration method with multigrid and multistep preconditioner. Acta Geotechnica, 19(10), 7011–7029. doi:10.1007/s11440-024-02414-9.

[5] Yang, H., Rahardjo, H., Leong, E. C., & Fredlund, D. G. (2004). Factors affecting drying and wetting soil-water characteristic curves of sandy soils. Canadian Geotechnical Journal, 41(5), 908–920. doi:10.1139/T04-042.

[6] Azizi, A., Jommi, C., & Musso, G. (2017). A water retention model accounting for the hysteresis induced by hydraulic and mechanical wetting-drying cycles. Computers and Geotechnics, 87, 86–98. doi:10.1016/j.compgeo.2017.02.003.

[7] Fu, Y., Xu, L., & Liao, H. (2024). Quantitative experimental study on the apparent contact angle of unsaturated loess and its application in soil–water characteristics curve modeling. Vadose Zone Journal, 23(6), 20376. doi:10.1002/vzj2.20376.

[8] Brooks, R. H. (1965). Hydraulic properties of porous media. PhD Thesis, Colorado State University, Fort Collins, United States.

[9] Brooks, R. H., & Corey, A. T. (1966). Properties of Porous Media Affecting Fluid Flow. Journal of the Irrigation and Drainage Division, 92(2), 61–88. doi:10.1061/jrcea4.0000425.

[10] Lyu, H., Fan, L., Gu, J., Huang, J., Chen, G., Shi, Z., & Zhang, J. (2024). Characterization of pore water distribution in unsaturated soils during drying process with NMR and soil-water characteristic curves. Transportation Geotechnics, 49, 101440. doi:10.1016/j.trgeo.2024.101440.

[11] Liu, H., Rahardjo, H., Satyanaga, A., & Du, H. (2023). Use of osmotic tensiometers in the determination of soil-water characteristic curves. Engineering Geology, 312, 106938. doi:10.1016/j.enggeo.2022.106938.

[12] Yan, G., Bore, T., Bhuyan, H., Schlaeger, S., & Scheuermann, A. (2022). The Technical Challenges for Applying Unsaturated Soil Sensors to Conduct Laboratory-Scale Seepage Experiments. Sensors, 22(10), 3724. doi:10.3390/s22103724.

[13] Kumar, A., Azizi, A., & Toll, D. G. (2022). Application of Suction Monitoring for Cyclic Triaxial Testing of Compacted Soils. Journal of Geotechnical and Geoenvironmental Engineering, 148(4), 4022009. doi:10.1061/(asce)gt.1943-5606.0002766.

[14] Abeykoon, T., Udukumburage, R. S., Gallage, C., & Uchimura, T. (2017). Comparison of direct and indirect measured soil-water characteristic curves for a silty sand. International Journal of GEOMATE, 13(39), 9–16. doi:10.21660/2017.39.170519.

[15] Fredlund, D. G., & Anqing Xing. (1994). Equations for the soil-water characteristic curve. Canadian Geotechnical Journal, 31(4), 521–532. doi:10.1139/t94-061.

[16] van Genuchten, M. T. (1980). A Closed- form Equation for Predicting the Hydraulic Conductivity of Unsaturated Soils. Soil Science Society of America Journal, 44(5), 892–898. doi:10.2136/sssaj1980.03615995004400050002x.

[17] Rossi, C., & Nimmo, J. R. (1994). Modeling of soil water retention from saturation to oven dryness. Water Resources Research, 30(3), 701–708. doi:10.1029/93WR03238.

[18] Assouline, S., Tessier, D., & Bruand, A. (1998). A conceptual model of the soil water retention curve. Water Resources Research, 34(2), 223–231. doi:10.1029/97WR03039.

[19] Aubertin, M., Mbonimpa, M., Bussière, B., & Chapuis, R. P. (2003). A model to predict the water retention curve from basic geotechnical properties. Canadian Geotechnical Journal, 40(6), 1104–1122. doi:10.1139/t03-054.

[20] Leong, E. C., & Rahardjo, H. (1997). Review of Soil-Water Characteristic Curve Equations. Journal of Geotechnical and Geoenvironmental Engineering, 123(12), 1106–1117. doi:10.1061/(asce)1090-0241(1997)123:12(1106).

[21] Dexter, A. R., Czyz, E. A., Richard, G., & Reszkowska, A. (2008). A user-friendly water retention function that takes account of the textural and structural pore spaces in soil. Geoderma, 143(3–4), 243–253. doi:10.1016/j.geoderma.2007.11.010.

[22] Omuto, C. T. (2009). Biexponential model for water retention characteristics. Geoderma, 149(3–4), 235–242. doi:10.1016/j.geoderma.2008.12.001.

[23] Khlosi, M., Cornelis, W. M., Douaik, A., van Genuchten, M. T., & Gabriels, D. (2008). Performance Evaluation of Models That Describe the Soil Water Retention Curve between Saturation and Oven Dryness. Vadose Zone Journal, 7(1), 87–96. doi:10.2136/vzj2007.0099.

[24] Cao, Y., Zhang, K., Liu, S., & Wang, Y. (2024). A review of advancements in the theory and characterization of soil macropore structure. PeerJ, 12(11), 18442. doi:10.7717/peerj.18442.

[25] Daneshian, B., Habibagahi, G., & Nikooee, E. (2021). Determination of unsaturated hydraulic conductivity of sandy soils: a new pore network approach. Acta Geotechnica, 16(2), 449–466. doi:10.1007/s11440-020-01088-3.

[26] Sharma, S., Rathor, A. P. S., & Sharma, J. K. (2025). Prediction of soil water characteristic curve of unsaturated soil using machine learning. Multiscale and Multidisciplinary Modeling, Experiments and Design, 8(1), 1–17. doi:10.1007/s41939-024-00664-4.

[27] He, X., Cai, G., & Sheng, D. (2025). Indirect models for SWCC parameters: reducing prediction uncertainty with machine learning. Computers and Geotechnics, 177, 106823. doi:10.1016/j.compgeo.2024.106823.

[28] Lee, T. D., & Yang, C. N. (1952). Statistical theory of equations of state and phase transitions. II. Lattice gas and ISING model. Physical Review, 87(3), 410–419. doi:10.1103/PhysRev.87.410.

[29] Hopfield, J. J. (2018). Neural networks and physical systems with emergent collective computational abilities. Feynman and Computation, 7–19. doi:10.1201/9780429500459.

[30] Strogatz, S. H. (2001). Exploring complex networks. Nature, 410(6825), 268–276. doi:10.1038/35065725.

[31] Goh, S., Choi, M. Y., Lee, K., & Kim, K. M. (2016). How complexity emerges in urban systems: Theory of urban morphology. Physical Review E, 93(5), 523091. doi:10.1103/PhysRevE.93.052309.

[32] Louf, R., Roth, C., & Barthelemy, M. (2014). Scaling in transportation networks. PLoS ONE, 9(7), 102007. doi:10.1371/journal.pone.0102007.

[33] Xu, J., & Louge, M. Y. (2015). Statistical mechanics of unsaturated porous media. Physical Review E - Statistical, Nonlinear, and Soft Matter Physics, 92(6), 0624051–06240517. doi:10.1103/PhysRevE.92.062405.

[34] Du, X., Du, C., Radolinski, J., Wang, Q., & Jian, J. (2022). Metropolis-Hastings Markov Chain Monte Carlo Approach to Simulate van Genuchten Model Parameters for Soil Water Retention Curve. Water (Switzerland), 14(12), 1968. doi:10.3390/w14121968.

[35] Chandler, D. (1987) Introduction to Modern Statistical Mechanics. Oxford University Press, Oxford, United Kingdom.

[36] Staple, W. J. (1962). Hysteresis Effects in Soil Moisture Movement. Canadian Journal of Soil Science, 42(2), 247–253. doi:10.4141/cjss62-033.

[37] Šimůnek, J., Kodešová, R., Gribb, M. M., & Van Genuchten, M. T. (1999). Estimating hysteresis in the soil water retention function from cone permeameter experiments. Water Resources Research, 35(5), 1329–1345. doi:10.1029/1998WR900110.

[38] Fatt, I., & Dykstra, H. (1951). Relative Permeability Studies. Journal of Petroleum Technology, 3(09), 249–256. doi:10.2118/951249-g.

[39] Mualem, Y. (1973). Modified approach to capillary hysteresis based on a similarity hypothesis. Water Resources Research, 9(5), 1324–1331. doi:10.1029/WR009i005p01324.

[40] Mualem, Y. (1974). A conceptual model of hysteresis. Water Resources Research, 10(3), 514–520. doi:10.1029/WR010i003p00514.

[41] Mualem, Y. (1984). A modified dependent-domain theory of hysteresis. Soil Science, 137(5), 283–291. doi:10.1097/00010694-198405000-00001.

[42] Mualem, Y., & Dagan, G. (1975). A dependent domain model of capillary hysteresis. Water Resources Research, 11(3), 452–460. doi:10.1029/WR011i003p00452.

[43] Klute, A., & Heermann, D. F. (1974). Soil water profile development under a periodic boundary condition. Soil Science, 117(5), 265–271. doi:10.1097/00010694-197405000-00005.

[44] Hoa, N. T., Gaudu, R., & Thirriot, C. (1977). Influence of the hysteresis effect on transient flows in saturated-unsaturated porous media. Water Resources Research, 13(6), 992–996. doi:10.1029/WR013i006p00992.

[45] Scott, P. S., Farquhar, G. J., & Kouwen, N. (1983). Hysteretic Effects on Net Infiltration. American Society of Agricultural Engineers, Michigan, United States.

[46] Kool, J. B., & Parker, J. C. (1987). Development and evaluation of closed- form expressions for hysteretic soil hydraulic properties. Water Resources Research, 23(1), 105–114. doi:10.1029/WR023i001p00105.

[47] Kool, J. B., & Parker, J. C. (1988). Analysis of the inverse problem for transient unsaturated flow. Water Resources Research, 24(6), 817–830. doi:10.1029/WR024i006p00817.

[48] Pot, V., Peth, S., Monga, O., Vogel, L. E., Genty, A., Garnier, P., Vieublé-Gonod, L., Ogurreck, M., Beckmann, F., & Baveye, P. C. (2015). Three-dimensional distribution of water and air in soil pores: Comparison of two-phase two-relaxation-times lattice-Boltzmann and morphological model outputs with synchrotron X-ray computed tomography data. Advances in Water Resources, 84, 87–102. doi:10.1016/j.advwatres.2015.08.006.

[49] Kaestner, A., Lehmann, E., & Stampanoni, M. (2008). Imaging and image processing in porous media research. Advances in Water Resources, 31(9), 1174–1187. doi:10.1016/j.advwatres.2008.01.022.

[50] Schlüter, S., Sheppard, A., Brown, K., & Wildenschild, D. (2014). Image processing of multiphase images obtained via X-ray microtomography: A review. Water Resources Research, 50(4), 3615–3639. doi:10.1002/2014WR015256.

[51] Chandler, R., Koplik, J., Lerman, K., & Willemsen, J. F. (1982). Capillary displacement and percolation in porous media. Journal of Fluid Mechanics, 119, 249–267. doi:10.1017/S0022112082001335.

[52] Brush, S. G. (1967). History of the Lenz-Ising model. Reviews of Modern Physics, 39(4), 883–893. doi:10.1103/RevModPhys.39.883.

[53] Christensen, K., & Moloney, N. R. (2005). Complexity and Criticality. Imperial College Press Advanced Physics Texts, World Scientific Publishing Company, Singapore. doi:10.1142/p365.

[54] Ng, C. W. W., & Pang, Y. W. (2000). Influence of Stress State on Soil-Water Characteristics and Slope Stability. Journal of Geotechnical and Geoenvironmental Engineering, 126(2), 157–166. doi:10.1061/(asce)1090-0241(2000)126:2(157).

[55] Roy, S., & Rajesh, S. (2018). Influence of Confining Pressure on Water Retention Characteristics of Compacted Soil. Indian Geotechnical Journal, 48(2), 327–341. doi:10.1007/s40098-017-0265-3.